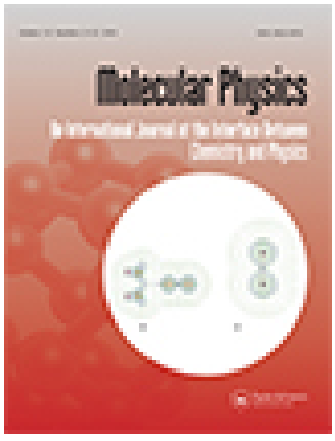

Molecular Physics: An International Journal at the Interface Between Chemistry and Physics
Publication details, including instructions for authors and subscription information:
http://www.tandfonline.com/loi/tmph20

Low-lying states of FeO and FeO^- by slow photoelectron spectroscopy

Jongjin B. Kim[a], Marissa L. Weichman[a] & Daniel M. Neumark[ab]
[a] Department of Chemistry, University of California, Berkeley, CA, USA
[b] Chemical Sciences Division, Lawrence Berkeley National Laboratory, Berkeley, CA, USA
Published online: 11 Feb 2015.

Molecular Physics, 2015
http://dx.doi.org/10.1080/00268976.2015.1005706

Taylor & Francis
Taylor & Francis Group

RESEARCH ARTICLE

Low-lying states of FeO and FeO^- by slow photoelectron spectroscopy

Jongjin B. Kim[a], Marissa L. Weichman[a] and Daniel M. Neumark[a,b,*]

[a]*Department of Chemistry, University of California, Berkeley, CA, USA;* [b]*Chemical Sciences Division, Lawrence Berkeley National Laboratory, Berkeley, CA, USA*

(*Received 20 November 2014; accepted 6 January 2015*)

High-resolution anion photoelectron spectra of FeO^- were acquired by slow electron velocity-map imaging of trapped and cooled ions. Ions were cooled to different temperatures by controlling the conditions in the trap, allowing us to disentangle contributions in the spectra from two different anion states. The spectra show that photodetachment of the two anion states accesses three low-lying neutral FeO states with one state in common, allowing us to derive term energies of all five states. The ground anion state is confirmed to be the $X\,^4\Delta$ state, and FeO is found to have an electron affinity of 1.4950 eV. We assign the anion $a\,^6\Sigma^+$ state, and obtain a term energy of 0.117 eV. The $A\,^5\Sigma^+$ and $a\,^7\Sigma^+$ neutral states are reassigned, and have term energies of 0.258 and 0.616 eV, respectively, relative to the neutral $X\,^5\Delta_4$ ground state.

Keywords: photoelectron; metal oxide; spectroscopy; iron

1. Introduction

Diatomic iron oxide, FeO, is a benchmark transition metal oxide. It serves as a fundamental system for understanding the complex chemical bonding between transition metals and oxygen atoms, an interaction that plays a key role in catalysis and other chemical processes. As such, FeO has been characterised by numerous spectroscopic methods, including matrix-isolation infrared absorption [1–3], rotational spectroscopy [4–6], Stark spectroscopy [7,8], anion photoelectron spectroscopy [9–12], and an array of absorption and emission spectroscopy techniques [13–20]; the results up to 1989 are summarised in a comprehensive review by Merer [21]. The corresponding anion FeO^- has been characterised indirectly from photoelectron spectroscopy [9–12] and autodetachment spectroscopy [22]. Here, we report new high-resolution anion photoelectron (PE) spectra combined with ion trapping and cooling. By comparison with previous *ab initio* calculations and new Franck–Condon (FC) simulations, we confirm the ground anion state and assign the first excited anion state as well as the lowest two neutral excited states.

The ground state of FeO has been confidently established as a $^5\Delta$ state by careful analysis of matrix-isolation IR spectra, gas-phase rotationally resolved IR absorption spectra, and visible emission spectra [21]. The ground state of FeO^- is less certain. By comparison of the anion PE spectrum to early FeO^- calculations, the anion ground state was assigned to a $^4\Delta$ state [9]. More concrete evidence for this assignment was provided by analysis of rotational and spin–orbit structure by autodetachment spectroscopy and anion zero electron kinetic energy (ZEKE) spectroscopy [12,22].

The properties and states of FeO and FeO^- have been studied by numerous *ab initio* [23–29] and density functional calculations [30–32]. Although there is an overall agreement that the ground state FeO is a quintet state, even high-level calculations disagree on whether the $^5\Sigma^+$ or $^5\Delta$ state is lower in energy, while the preponderance of experimental evidence is in favour of the $^5\Delta$ state. A low-lying $^7\Sigma^+$ excited state is also expected. For the FeO^- anion, recent *ab initio* calculations have suggested a $^6\Sigma^+$ ground state [28,29], and while the ZEKE and autodetachment analyses argue strongly in favour of a $^4\Delta$ state, not all features in these spectra are fully understood, leaving some uncertainty in the experimental assignments [33].

The low-lying excited states of FeO and FeO^- are less well characterised experimentally and theoretically. While optical spectroscopic techniques have probed and assigned various states of FeO lying $\sim 10^4$ cm^{-1} above the ground state, these experiments could not directly probe any lower lying excited states. Electronic structure calculations have suggested the existence of low-lying $^5\Sigma^+$ and $^7\Sigma^+$ states. However, the $^7\Sigma^+$–$^5\Delta$ transition is spin-forbidden, the $^5\Sigma^+$–$^5\Delta$ transition is dipole forbidden, and allowed transitions to the $^5\Sigma^+$ state from other states are calculated to have weak intensity [24]. Anion photoelectron spectroscopy provides an alternative means to probe the electronic states of FeO owing to its different selection rules. The PE spectrum reported by Engelking was assigned to transitions

* Corresponding author. Email: dneumark@berkeley.edu

from the anion $^4\Delta$ state to the ground $^5\Delta$ and excited $^5\Sigma^+$ states of FeO [9]. Subsequent work at higher photon energies revealed more FeO excited states [10,11]. Anion ZEKE spectra showed additional features tentatively assigned to the neutral $^7\Sigma^+$ state [12], though such a transition from the anion $^4\Delta$ state should be forbidden [33].

Excited electronic states of the FeO^- anion were investigated by autodetachment spectroscopy, which identified several dipole-bound and valence states near the adiabatic detachment energy of 1.49 eV [22]. Only tentative assignments were made for those states. No technique has probed lower lying states of the anion, though the differing experimental and theoretical results for the ground state assignment suggest that there should be at least one low-lying excited state. Electronic structure calculations have found low-lying $^4\Delta$, $^6\Sigma^+$, and $^6\Delta$ states, with either the $^4\Delta$ or $^6\Sigma^+$ as the ground state [28–30]. Identifying one of these as an excited state would help confirm the identity of the ground state. Overall, additional experimental data are needed to confidently establish the nature and energetics of the low-lying states of FeO and FeO^-.

We report new high-resolution PE spectra of the FeO ← FeO^- transitions with slow electron velocity-map imaging (SEVI), a technique that is more flexible than anion ZEKE with only a slight loss in resolution [34], combined with ion trapping and cooling, which allows for more control over ion temperatures compared to the standard free gas jet expansion methods [35]. For this system, we acquire sub-meV to meV-resolution PE spectra with different ion temperatures, allowing us to separate different contributions from two different anion states and to partially reassign the PE spectra as detachment from two low-lying anion states to three low-lying neutral states. We confirm the ground state assignments of $X\,^4\Delta$ and $X\,^5\Delta$ for the anion and neutral FeO, but reassign the $A\,^5\Sigma^+$ and $a\,^7\Sigma^+$ neutral states and assign the $a\,^6\Sigma^+$ anion state for the first time. The assignments are corroborated with electronic structure considerations, FC simulations, threshold intensity trends, and PE anisotropies. We obtain term energies for all states relative to each other with meV precision, and provide a consistent description for all low-lying states.

2. Experimental methods

Our experimental apparatus has been described in detail previously [34–36]. Iron oxide anions were generated by laser ablation, stored in a temperature-controlled ion trap, mass-selected, and photodetached. The PEs were analysed by SEVI, with the possibility of acquiring either high-resolution spectra over a narrow region per scan or low-resolution spectra spanning several thousand cm^{-1} per scan.

FeO^- anions were generated by laser ablation of a steel target by a 2–10 mJ pulse of 532 nm focused laser light, quenched by a pulse of helium and trace oxygen. The anions were transferred by ion guides to an octopole ion trap. The ion trap was held either at 10 or 300 K and filled with buffer gas of helium or a 1:4 mix of H_2:He gas.

The ions were extracted from the ion trap, mass-selected in a time-of-flight spectrometer, and directed to a velocity-map imaging (VMI) electron spectrometer [37], where $^{56}Fe^{16}O^-$ ions were detached by the tunable output from a pulsed dye laser. The VMI electrostatic lens projected the PE distribution onto a planar position-sensitive detector, which counted individual PE events [38]. The original PE radial distribution was reconstructed from the projected image [39].

Under VMI focusing conditions, the radius of the distribution is proportional to the electron speed, and thus the electron kinetic energy (eKE) spectrum can be constructed from the PE image. As described in detail previously [40], we acquire the highest energy resolution at lowest eKE, and thus high-resolution spectra are acquired by splicing together low-eKE segments of spectra acquired at various photon energies, and roughly scaling them to match the intensities in a low-resolution, wide-energy overview scan. As detachment photon energies are varied, we report spectra in eBE, defined as the energy between the anion and neutral states and derived from the eKE spectra by the relation $\mathrm{eBE} = h\nu - \mathrm{eKE}$.

The photoelectron angular distributions (PADs) are also acquired by the electron images. They can be parameterised by a single quantity β, for the case of a single-photon detachment by linearly polarised light [41,42]. The value of β ranges from -1 to 2, for the limits of a PAD aligned perpendicular and parallel to the polarisation axis, while a value of 0 corresponds to an isotropic distribution. For a given detachment transition, the value of β is a function of eKE, and hence a single numerical value cannot be assigned for each transition [41,43]. However, the qualitative behaviour of β as a function of eKE is often characteristic of a given electronic transition [44].

3. Results

SEVI spectra taken under differing conditions are shown in Figures 1–3. The spectra shown in Figure 1 are for ions cooled in a 10 K ion trap with the H_2/He buffer gas mix at an estimated pressure of $\sim 10^{-4}$ torr in the trap, and show both lower resolution overview spectra and high-resolution scans. Figure 2(a) shows overview spectra of ions stored in a trap held at room temperature using the same buffer gas mix; the buffer gas pressure is varied between an estimated $\sim 10^{-5}$ and 10^{-4} torr in the trap to control the cooling efficiency, as there is incomplete thermalisation at lower trap gas densities. Figure 3 shows overview and high-resolution spectra acquired of ions stored in a 10 K ion trap, but with helium-only buffer gas, also at an estimated trap pressure $\sim 10^{-4}$ torr.

Previous experiments with our instrument have found that the H_2/He buffer gas mix is effective at cooling the

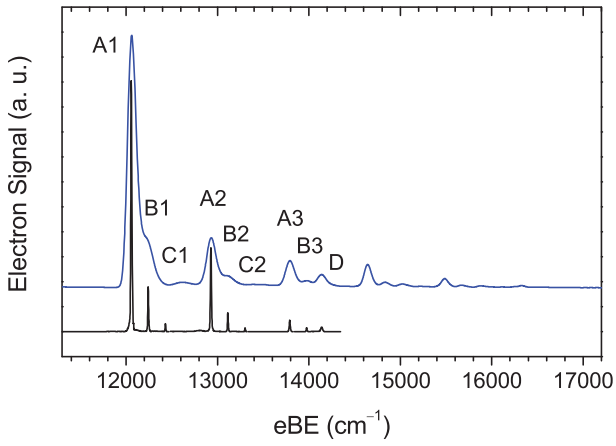

Figure 1. SEVI spectra of FeO^- under the coldest conditions, with a H_2/He buffer gas mix and a 10 K trap. The upper blue trace is an overview spectrum taken near photon energies of 17,745 cm^{-1}. The bottom black traces are high-resolution portions of scans taken at lower photon energies.

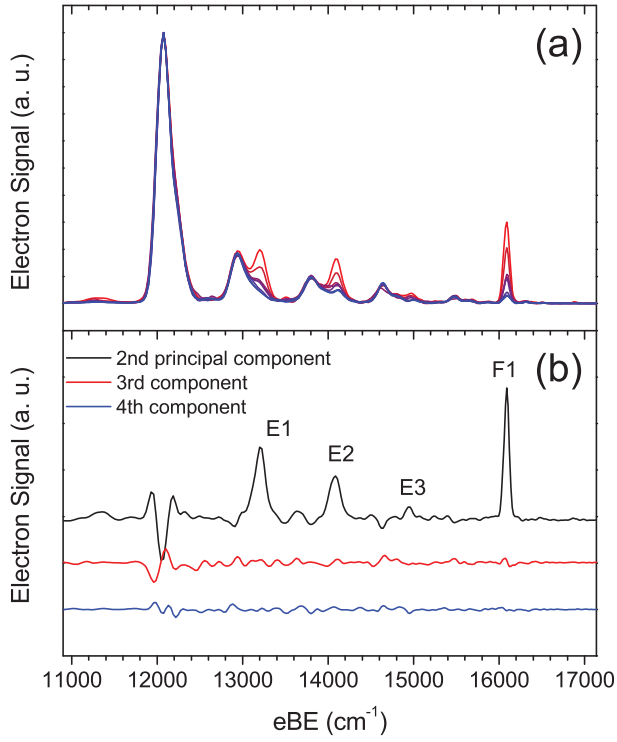

Figure 2. PE spectra of FeO^- taken with a H_2/He buffer gas mix and a trap temperature of 300 K. Panel (a) shows the experimental spectra taken at photon energies of 17,745 cm^{-1}. The trap buffer gas pressure is varied, from lowest (red) to highest (blue). Panel (b) shows the first several principal components of the set of spectra. The first component is just the average of the spectra and is omitted.

rovibronic degrees of freedom in anions, with internal temperatures as low as 10 K achieved at a trap temperature of 5 K [35]. However, helium by itself can be much less effective at cooling ions. For example, we observed a vibrational temperature of ~450 K for S_3^- in He buffer gas at an ion trap temperature of 35 K, whereas vibrational hot bands were eliminated by replacing He with H_2 [45]. We expect the spectra in Figure 1 to represent those of ions with all degrees of freedom cooled to approximately 10 K, while those in Figure 2 are from ions that should approach a temperature of 300 K as the trap gas pressure is increased. Under the conditions relevant to Figure 3, there can be substantial vibrational and possibly electronic excitation in the ions, depending on their energy distribution coming out of the laser ablation source and the effectiveness of collisional energy transfer from the various degrees of freedom to He.

The spectra of FeO^- under cold conditions (Figure 1) have a strong vibrational origin peak A1. There are two characteristic peak spacings: an ~870 cm^{-1} progression composed of peaks A1, A2, etc., and ~190 cm^{-1} progressions (A1, B1, C1), (A2, B2, C2), and (A3, B3). Peak D does not fall under one of the latter progressions; its position is 25 cm^{-1} above the extrapolated peak C3 position, a discrepancy beyond the instrumental resolution. Moreover, its intensity in the overview spectrum is larger than what should be the more intense peak B3. It thus appears to be associated with a different electronic transition. No other structure is apparent in the energy range 10,000–17,700 cm^{-1}; peak positions under 'cold' conditions are listed in Table 1.

The spectra in Figure 2(a) are all overview spectra taken at photon energies of 17,745 cm^{-1}. Qualitatively, the observed structure in these spectra is similar to that in the overview spectrum in Figure 1. However, the individual peaks are less distinct. New peaks also appear around 13,200, 14,100, 15,000, and 16,100 cm^{-1}. The intensities of these peaks diminish as the density of buffer gas increases (red to blue traces), but not entirely, even at the highest buffer gas concentrations. These peaks are more clearly seen as the second component in a principal component analysis of the set of spectra (Figure 2(b)) [46]. In this analysis, the variance in the data is decomposed as a set of eigenvectors (principal components), in the order of decreasing contribution to the variance; the first component is simply an average of the different spectra, but higher components show which parts of the spectra track together upon changes in ion cooling conditions. Peaks E1–E3 and F1 are prominent in the second principal component and are absent in higher components, indicating that their intensities track together with varying ion cooling. There is also some structure in Figure 2(b) associated with the lowest eBE peak resulting from shifting of this feature with temperature. Peaks E1–E3 are spaced by ~900 cm^{-1}, characteristic of a vibrational progression, and the strong onset of peak E1 in this progression suggests that it is the vibrational origin of an electronic transition. Peak F1 is offset from E1 by 2891 cm^{-1}, much too large for a vibrational excitation, and suggests the origin of another electronic transition.

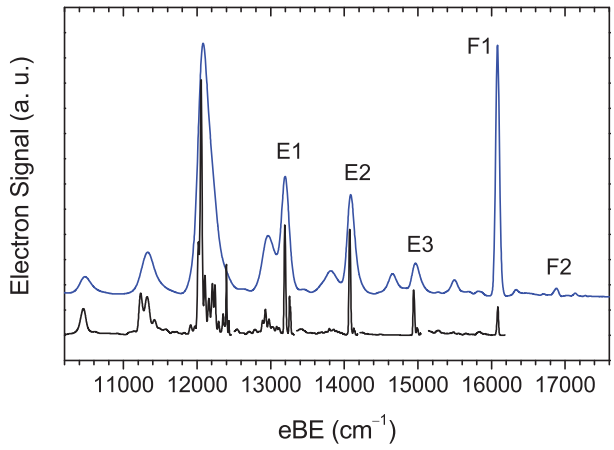

Figure 3. SEVI spectra of FeO^- with a 10 K trap but with only helium buffer gas. The upper blue trace is an overview spectrum taken at photon energy of 17,745 cm^{-1}, while the lower black traces are high-resolution portions of scans taken at lower photon energies.

Spectra taken with pure helium buffer gas show even more structure (Figure 3), suggesting considerable excitation in the anions under these conditions. All features in the room temperature spectra are present, with peaks E1–F1 even more intense in spectra acquired at the same photon energy. High-resolution scans of those peaks give the peak positions reported in Table 1 under 'hot' conditions. Peak F2 lies above peak F1 by ~790 cm^{-1}, and is likely offset by a vibrational quantum. Below ~13,000 cm^{-1}, the spectra are congested. Moreover, prominent peaks appear below 12,000 cm^{-1}, a spectral region with little or no signal in Figures 1 and 2. Relative peak intensities vary noticeably with the photon energies used, likely due to contributions from autodetachment below 13,000 cm^{-1} [22]. Peaks are neither assigned nor labelled in this region. A progression with an approximate peak spacing of ~800 cm^{-1} extends below peak A1, but well-resolved spectra were not acquired for these peaks.

Anisotropy parameters β for the PADs of several peaks are shown in Figure 4 as a function of eKE. PADs for the peaks in the cold spectra except for peak D are shown in panel (a), while those of peak D and all other peaks are shown in panel (b). We estimate errors of β to be around 0.1. Peaks E1–F1 exhibit a well-ordered rise in β with eKE, levelling off at $\beta \approx 1$. Peak D exhibits a slow decline in β, and is negative at high eKE, unlike all other peaks. Peaks A1–B3 also have positive β at large eKE.

Almost all peaks retain appreciable intensities near threshold, where the eKE is at or below ~100 cm^{-1}. However, peaks D, F1, and F2 all have small intensities at low eKE. Assuming the cross section of the high eKE peak A1 changes very little with photon energy, we can roughly normalise the intensities of low eKE peaks to A1 over a narrow range. The relative intensities of peaks D and F1 go as $\sigma \propto eKE^{1.6}$ and $\sigma \propto eKE^{0.97}$ in a power-law fit for eKE < 400 cm^{-1}, respectively. The intensity of peak F2 was too small for an analogous determination of the eKE dependence. In comparison, as an exemplar of the main band, peak A2 goes as $\sigma \propto eKE^{0.21}$. Peaks E1–E3 have significant intensity near threshold, but there are insufficient scans at various photon energies for a similar eKE-dependence analysis.

Table 1. Peak positions (cm^{-1}) compared to those from previous work, shifts from the origin (cm^{-1}), and assignments for the FeO^- SEVI spectra with the peaks that only appear under cold conditions and the most prominent peaks that appear under hotter ion conditions.

Peak	eBE	Drechsler et al.[a]	Offset	Electronic	Vibrational
			Cold		
A1	12,058	12,054	0	$X\,^5\Delta_4 \leftarrow X\,^4\Delta_{7/2}$	0–0
B1	12,242	12,243	185	$X\,^5\Delta_3 \leftarrow X\,^4\Delta_{7/2}$	0–0
C1	12,431	12,435	373	$X\,^5\Delta_2 \leftarrow X\,^4\Delta_{7/2}$	0–0
A2	12,929	12,928	871	$X\,^5\Delta_4 \leftarrow X\,^4\Delta_{7/2}$	1–0
B2	13,114	13,117	1056	$X\,^5\Delta_3 \leftarrow X\,^4\Delta_{7/2}$	1–0
C2	13,301	13,310	1243	$X\,^5\Delta_2 \leftarrow X\,^4\Delta_{7/2}$	1–0
A3	13,790	13,795	1733	$X\,^5\Delta_4 \leftarrow X\,^4\Delta_{7/2}$	2–0
B3	13,975		1917	$X\,^5\Delta_3 \leftarrow X\,^4\Delta_{7/2}$	2–0
D	14,139		2082	$A\,^5\Sigma^+ \leftarrow X\,^4\Delta_{7/2}$	0–0
			Hot		
E1	13,194	13,198	1136	$A\,^5\Sigma^+ \leftarrow a\,^6\Sigma^+$	0–0
E2	14,074	14,080	2016	$A\,^5\Sigma^+ \leftarrow a\,^6\Sigma^+$	1–0
E3	14,945	14,957	2887	$A\,^5\Sigma^+ \leftarrow a\,^6\Sigma^+$	2–0
F1	16,083	16,100[b]	4025	$a\,^7\Sigma^+ \leftarrow a\,^6\Sigma^+$	0–0
F2	16,876	16,900[b]	4818	$a\,^7\Sigma^+ \leftarrow a\,^6\Sigma^+$	1–0

[a][12].
[b]Values from time-of-flight (TOF) PE spectroscopy. All other values from Drechsler et al. [12] are from anion ZEKE.

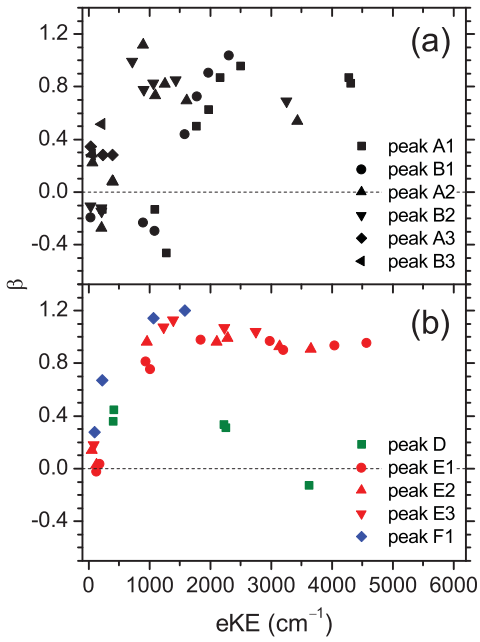

Figure 4. PADs for most peaks as a function of eKE. Panel (a) shows those of the ground-state band, while panel (b) shows those of the other electronic transitions. Peaks with a common electronic transition are labelled with the same colour.

Peak positions and assignments are summarised in Table 1. Peaks are wider than in previous SEVI spectra due to unresolved rotational structure, as well as small intensities near threshold for peaks D and F2, requiring the use of higher eKE spectra for those features. No substructure is visible for most peaks. For those, we conservatively report peak position errors by a standard deviation of a Gaussian fit to each peak: 4–6 cm^{-1} for peaks A1–B3, 10 cm^{-1} for peak D, and 31 cm^{-1} for peak F2. The highest resolution spectra for peaks E1–F1 using pure He buffer gas show a double-peak structure (not shown); for the assigned photodetachment transitions (Section 5.2), we expect these to correspond to partially resolved P and R branches, and fitting this feature allows for more precise peak positions [47,48]. Using bond lengths from the calculations used in the FC simulations (see below) and convoluting simulated rotational structure with the instrumental resolution, we obtain peak positions for E1–F1 by the rotational profile fit. For these peaks, we report errors as the instrumental resolution of the scans, 4 cm^{-1}.

4. Franck–Condon simulations

To aid in the assignment of the various bands, we compare the experimental spectra with FC simulations of the likely photodetachment transitions. We considered all possible photodetachment transitions from the three calculated lowest lying anion states ($^4\Delta$, $^6\Sigma^+$, $^6\Delta$) to the lowest three neutral states ($^5\Delta$, $^5\Sigma^+$, $^7\Sigma^+$). We used frequencies and geometries from previously published *ab initio* calculations for all six states to calculate the FC simulations. To check for consistency with different methods, we used results from CASPT2 [28], as well as MRCI + Q and RCCSD(T) with scalar relativistic correction [29]. All three methods give qualitatively similar FC simulations, even though the relative state energies depend on the method.

FC intensities were calculated within the harmonic oscillator approximation using the ezSpectrum program [49]. Calculated FC intensities for all nine detachment transitions with all three methods are displayed in Figure 5. As there is only one vibrational degree of freedom, FC intensities are shown as a function of vibrational quantum number v rather than energy to facilitate comparison between different electronic structure methods and states. Based on the electron orbital configurations for these states [21,23,25,28,29], the corresponding detachment transitions are also overlaid for convenience, with two-electron transitions shown lighter. Representative orbital pictures can be found in CASSCF calculations by Hendrickx and Anam [28], and are qualitatively similar to descriptions in other *ab initio* studies [23,29].

5. Discussion

5.1. Assignment of cold spectra

Peak A1 is assigned the vibrational origin of the $X\,^5\Delta_4 \leftarrow X\,^4\Delta_{7/2}$ transition. The progressions A1, A2, A3 and A1, B1, C1 can be readily assigned to vibrational and spin–orbit structure, with characteristic peak spacings of ~870 cm^{-1} and 190 cm^{-1}, respectively, in excellent agreement with the literature values for the energy spacings of both components (Table 2). Peak positions are also close to the values from anion ZEKE spectra reported by Drechsler et al. [12], who assigned the peaks in the same manner (Table 1). However, as we cool the ions in a cryogenic trap, we do not see any contributions from excited anion spin–orbit components, ensuring that the ions are in their $X\,^4\Delta_{7/2}$ ground state. FC simulations are also consistent with this assignment. For a $^5\Delta \leftarrow {}^4\Delta$ transition, the origin is expected to be strong with minor vibrational activity (Figure 5), as is also seen in the spectra.

The PADs have not been measured before, and are consistent with this assignment. The $^5\Delta \leftarrow {}^4\Delta$ transition involves detachment from a σ orbital; as the Σ^+ irreducible representation describes both s and p orbitals, we would expect contributions from both $l = 0$ and $l = 1$ partial waves, i.e. s- and p-wave detachment. In the atomic limit, detachment from a p orbital would be expected to have a near-zero β, while an s orbital would be expected to have a positive β; the superposition of these two contributions would likely yield a positive β, as we see for peaks A1–B3. According the Wigner Threshold law, threshold photodetachment intensities should scale as eKE$^{l+1/2}$ [50]. We observe threshold scaling of $\sigma \propto$ eKE$^{0.21}$ for these peaks.

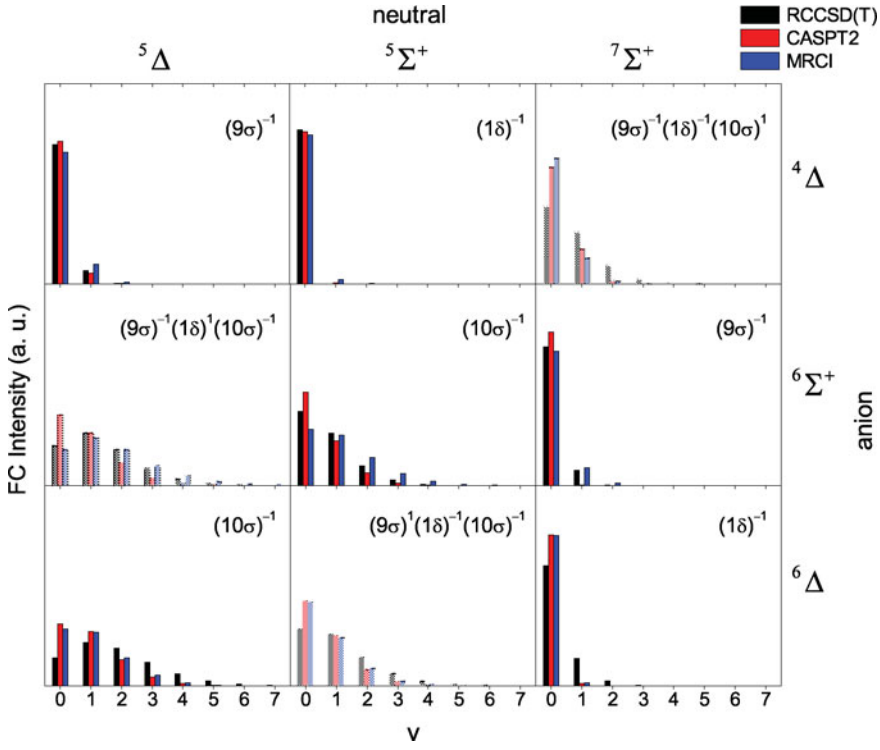

Figure 5. Franck–Condon (FC) simulations between the possible low-lying states of FeO^- and FeO, using the calculated geometries and harmonic frequencies of previous *ab initio* reports as described in Section 4. As there is only one vibrational degree of freedom, stick spectra are given as a function of vibrational quantum number and not energy. Semitransparent graphs correspond to two-electron transitions, and the detachment orbital transitions are labelled for each panel. FC intensities are normalised to the same integral intensities over a given electronic transition.

This scaling is steeper than even with a wholly *s*-wave detachment with $\sigma \propto eKE^{0.5}$. Such a result may reflect the long-range dipole interaction between the neutral FeO and a departing electron, which can reduce the eKE exponent and cause a steeper increase of cross section with eKE [51,52].

Peak D has not been seen in previous photodetachment experiments. Although superficially it would appear to correspond to a peak C3 by extrapolation, neither the peak intensity nor peak position matches the expectation. Moreover, the PAD and threshold intensity behaviour differs from all other peaks; the value of β decreases with increasing eKE instead of rising to a value near 0.8, and it has vanishing intensity near threshold, with $\sigma \propto eKE^{1.6}$. These considerations suggest that peak D is from a different photodetachment transition than all the other observed peaks in Figure 1.

As we have already assigned the $^5\Delta \leftarrow {}^4\Delta$ band, with H_2/He buffer gas at 10 K, we can assume that all the anions

Table 2. Term energies and vibrational fundamentals compared to the literature values.

	State		cm^{-1}	eV	Merer[a]	Drechsler et al.[b]
FeO	$X\,^5\Delta_4$	EA	12,058(6)	1.4950(7)		12,054
		$\Delta G_{1/2}$	871(6)		871.152	874
		$^5\Delta_3$–$^5\Delta_4$	185(4)		184.084	189
		$^5\Delta_2$–$^5\Delta_3$	189(4)		188.177	192
	$A\,^5\Sigma^+$	T_0	2082(10)	0.258(1)		
		$\Delta G_{1/2}$	880(4)			882[c]
	$a\,^7\Sigma^+$	T_0	4971(10)	0.616(1)		
		$\Delta G_{1/2}$	793(31)			800[c,d]
FeO^-	$a\,^6\Sigma^+$	T_0	945(10)	0.117(1)		

[a][21].
[b][12].
[c]Vibrational frequencies are those that would be obtained reassigning their states to match ours.
[d]From TOF PE spectroscopy.

are in the $^4\Delta$ ground state. Thus, there are only two other transitions to consider, those from the $^4\Delta$ anion state to the $^5\Sigma^+$ and $^7\Sigma^+$ neutral states. The $^7\Sigma^+ \leftarrow {}^4\Delta$ transition is formally a forbidden two-electron transition, and furthermore requires a spin flip. The $^5\Sigma^+ \leftarrow {}^4\Delta$ transition is an allowed one-electron transition involving detachment of an electron from a δ orbital. We therefore assign peak D to the vibrational origin of the $A\,^5\Sigma^+ \leftarrow X\,^4\Delta_{7/2}$ band.

FC simulations support this assignment. The simulated FC structure for the $^7\Sigma^+ \leftarrow {}^4\Delta$ transition predicts significant vibrational activity, with the $v = 1$ transition having $\sim$1/3 the intensity of the origin. While the experimental intensity of peak D is weak, other spectra at higher photon energies (not shown) show no evidence of any appreciable FC intensity beyond peak D that cannot be assigned to the $^5\Delta \leftarrow {}^4\Delta$ band. This result does not match the predicted FC profile of the $^7\Sigma^+ \leftarrow {}^4\Delta$ transition, but is compatible with the $^5\Sigma^+ \leftarrow {}^4\Delta$ transition, which predicts almost all FC intensity in the origin.

The PADs and threshold intensities are also consistent with this assignment. The value of β for peak D decreases with increasing eKE, and its threshold intensity scales as $\text{eKE}^{1.6}$. This behaviour is characteristic of a transition with p-wave detachment from a δ orbital. Though the PAD is not a definitive signature of a particular transition, PADs with negative values of β are characteristic of detachment from a p or d orbital in the limit of detachment from an atomic centre [53]. Assuming a single partial-wave contribution, the observed threshold scaling gives $l = 1$, which can be achieved by detachment of an s or d orbital in the atomic limit; for detachment to a Σ state, the long-range dipole interaction should not affect this model, according to the treatment by Engelking [51]. Based on these characteristics, peak D would seem to result from a d orbital centred on the iron atom. This matches the assignment of detachment from a 1δ orbital; by symmetry, the 1δ orbitals do not interact with the valence oxygen orbitals and remain almost purely single-centre d orbitals. The assignment of 1δ detachment is also consistent with the small intensity of peak D even at large eKE, as discussed in Section 5.3.

5.2. *Assignment of warmer spectra*

Having assigned the features in the cold spectra, we can now understand the additional features that appear under warmer conditions. At room temperature, as the buffer gas density changes, the relative intensities of peak E1–F1 in Figure 2 change in concert, suggesting that they arise by detachment from a common anion state. These features are even more intense when the ions are trapped and inefficiently cooled (Figure 3). Based on the strong intensities relative to each other and with respect to the ground-state transition, these two bands are likely one-electron-allowed transitions from a common anion state to two different neutral states.

Since the anion ground state is established to be a $^4\Delta$ state, the possible anion states are the $^6\Sigma^+$ and $^6\Delta$ states. The allowed transitions from the $^6\Sigma^+$ state are to the $^5\Sigma^+$ and $^7\Sigma^+$ states, with detachment from the 10σ and 9σ orbitals, respectively. The allowed transitions from the $^6\Delta$ state are to the $^5\Delta$ and $^7\Sigma^+$ states, with 10σ and 1δ orbital detachment. The neutral ground state is the $^5\Delta$ state; so, if the $^6\Delta$ state was populated, we would expect to see a band below peak A1, which does not correspond to bands E and F, though it may contribute to the spectrum in Figure 3 (see below). Thus, bands E and F occur by detachment from the $^6\Sigma^+$ anion state. As peak E1 but not F1 is lower in energy than peak D, band E likely corresponds to the $^5\Sigma^+ \leftarrow {}^6\Sigma^+$ transition while band F corresponds to the $^7\Sigma^+ \leftarrow {}^6\Sigma^+$ transition.

The FC simulations and PADs support this assignment. The simulated $^5\Sigma^+ \leftarrow {}^6\Sigma^+$ spectrum shows significant FC activity; though the origin is the most intense peak, there is significant intensity out to $v = 2$, in good correspondence with peaks E1–E3. In contrast, the simulated $^7\Sigma^+ \leftarrow {}^6\Sigma^+$ spectrum is dominated by the vibrational origin, with weak $v = 1$ activity, similar in appearance to peaks F1 and F2. The PADs for both bands are characterised by a positive β. As noted in the previous section, this would correspond to σ orbital detachment, consistent with these 9σ and 10σ detachment transitions. Bands E and F are thus assigned to the $A\,^5\Sigma^+ \leftarrow a\,^6\Sigma^+$ and $a\,^7\Sigma^+ \leftarrow a\,^6\Sigma^+$ transitions. Full assignments of all peaks are listed in Table 1.

Curiously, though both bands E and F have detachment from a σ orbital, they exhibit different threshold behaviour. Band E has appreciable threshold intensity in our spectra, but band F has little threshold intensity, and a power-law fit with eKE gives threshold intensity as $\text{eKE}^{0.97}$. As the neutral states are Σ states, the dipole moment should not influence the Wigner threshold expression [51]. This value does not correspond to a single l value in the Wigner threshold expression, and is likely better expressed as a combination of s- and p-wave contributions, though the few data points available make a reliable decomposition unreliable. Detachment from the 1δ orbital should give $\sigma \propto \text{eKE}^{1.5}$ as explained earlier, but both bands E and F are inconsistent with this behaviour and more consistent with that of σ detachment.

With the spectra under warmer conditions assigned, we can compare the cooling efficiency between He and H_2/He buffer gas. Vibronic cooling is inefficient using pure He, with significant population of the $a\,^6\Sigma^+$ anion state 0.117 eV above the ground state (see below). However, rotational cooling is effective in both buffer gas environments. The rotational fit for the $A\,^5\Sigma^+ \leftarrow a\,^6\Sigma^+$ and $a\,^7\Sigma^+ \leftarrow a\,^6\Sigma^+$ transitions yield an anion rotational temperature of 40 ± 5 K for the $a\,^6\Sigma^+$ state with He gas cooling. A similar rotational fit can be made for the features seen with H_2/He buffer gas; though since there is no substructure seen for these, the fit is far less reliable. For the $X\,^5\Delta \leftarrow X\,^4\Delta_{7/2}$ transitions under

these conditions, we can use a similar treatment [48], and we obtain an anion rotational temperature of 20 ± 10 K. Unsurprisingly, this is lower than the temperatures with only a He buffer gas, but both are comparably cold. As has been observed in free jet experiments, the rotational temperature equilibrates before the vibronic degrees of freedom.

5.3. *Electronic states of FeO and FeO⁻*

Under the coldest ion conditions here, all observed features can be assigned due to detachment from a $^4\Delta$ anion state. The anion ZEKE and autodetachment spectra both supported the assignment of a $^4\Delta$ ground state with their rotationally resolved structure [12,22,33], but there were anomalous features in the ZEKE spectra and only portions of the autodetachment spectra were successfully assigned. Furthermore, *ab initio* calculations have suggested that the $^6\Sigma^+$ state is the ground state [28,29]. While our experiment does not improve on the ZEKE study in resolution, our additional flexibility and ion temperature control allow us to explain anomalies in previous spectra. With a consistent explanation for all observed features, we can confirm that the ground-state anion is a $^4\Delta$ state. Establishing this state allows us to determine the nature and energetics of the other states observed.

Although the assignment of peak D to the origin of the $A\ ^5\Sigma^+ \leftarrow X\ ^4\Delta$ band is consistent with electronic configurations, FC profiles, threshold intensities, and PADs, this peak has not been seen in earlier work. In previous PE spectra, the resolution was insufficient to observe the spin–orbit $^5\Delta$ structure; similarly, the resolution would be insufficient to resolve peak D [9–11]. The high-resolution ZEKE spectrum, though it had sufficient resolution, also did not reveal such a feature [12]; As peak D appears to obey *p*-wave detachment, it has vanishing intensity near threshold and thus cannot be detected by ZEKE, which discriminates against such features. The flexibility of SEVI allows for well-resolved spectra of detachment features with *p*-wave character.

The intensity of peak D is surprisingly small even far from threshold, compared to the relatively larger intensities of the other three detachment transitions. This transition comes by detachment from a 1δ orbital, while the other transitions have detachment from the 9σ or 10σ orbitals. Calculating the cross sections quantitatively is beyond the scope of this work [54], but we can use empirical experimental cross sections of simpler species for a qualitative comparison. For the first-row transition metal atoms, the cross sections of 3*d* orbital detachment are significantly smaller than those of 4*s* detachment [55,56]. Thus, it would seem reasonable that 1δ detachment from a purely Fe 3*d* orbital would have smaller intensities than 9σ and 10σ detachment from orbitals with significant Fe 4*s* character. This small intensity likely has been a factor in peak D not being resolved until now.

While peak D had not been observed in earlier photodetachment experiments, it was noted that emission spectra of FeO exhibited perturbations ~2100 cm^{-1} above the ground state, a value very similar to our assignment of 2082 cm^{-1} for the $A\ ^5\Sigma^+$ state [19]. Based on the parity selection of the perturbations, they were attributed to a nearby Σ state. Since the $^5\Sigma^+$ state was assigned in a previous photodetachment experiment [9], the perturbing state was assigned to the next likely candidate, the $^7\Sigma^+$ state. However, with our reassignment of the PE spectra, this feature corresponds well with our peak D, and is consistent with our assignment of a $^5\Sigma^+$ state.

This assignment also allows us to determine the term energy of the $a\ ^6\Sigma^+$ anion state. Both the $X\ ^4\Delta$ and $a\ ^6\Sigma^+$ states can detach to the $A\ ^5\Sigma^+$ state of FeO, and the term energy can be determined by the difference of the corresponding detachment energies, peaks D and E1. Similarly, the term energy of the $a\ ^7\Sigma^+$ state can be derived relative to the neutral $X\ ^5\Delta$ state, as we measure the energies of the transitions in Figure 6, which connect all the states we probe. The weak peak D assigned to the $A\ ^5\Sigma^+ \leftarrow X\ ^4\Delta$ transition is the key feature in our data that allows us to connect all five states. We derive term energies of 0.117 and 0.616 eV for the $a\ ^6\Sigma^+$ and $a\ ^7\Sigma^+$ states relative to the anion and neutral ground states, respectively. The error of these energies is limited by the relatively large uncertainty of 10 cm^{-1} for peak D. Term energies and vibrational frequencies of the various states are summarised in Table 2.

This term energy for the $a\ ^6\Sigma^+$ state derived by energy balance is consistent with the observed structure in the room-temperature spectra. In those spectra, as the buffer gas density increases, the intensities of bands E and F diminish, but even at the highest gas densities used, peak F1

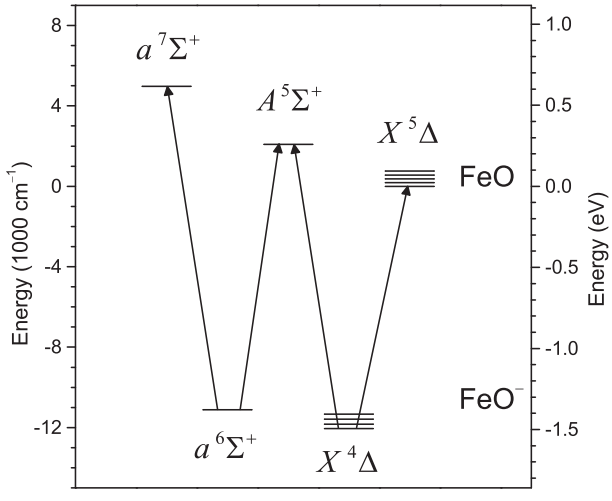

Figure 6. Energy level diagram showing the four detachment transitions assigned in this work. Energies are relative to the $X\ ^5\Delta_4$ level, and are from this work, save for the spin–orbit multiplet structures of the $^5\Delta$ and $^4\Delta$ states, which are from the literature values.[12,21]

has measureable intensity, with an integrated intensity ≈1% that of the ground-state transitions. Assuming roughly similar photodetachment cross sections would imply a ∼1% population of the $^6\Sigma^+$ state at room temperature. Further assuming that the only states of concern are the $^4\Delta$ multiplet and the $^6\Sigma^+$ state, with similar rotational and vibrational partition functions, we can consider this as a five-level system with only the term energy of the $^6\Sigma^+$ as a free parameter, as the spin–orbit splitting of the $^4\Delta$ state is known [12,22]. Putting bounds of a 0.3–3.0% population, we derive a likely energy range of 0.08–0.14 eV for the term energy of the $a\,^6\Sigma^+$ state relative to the $X\,^4\Delta_{7/2}$ state. These bounds agree with the more precise value of 0.117 eV derived above; this self-consistency further suggests that these two different anion states access the same neutral state in peaks D and E1–E3.

Assignments of the $A\,^5\Sigma^+$ and $a\,^7\Sigma^+$ states, while consistent with the experimental results in this report, differ from assignments in previous photodetachment experiments. All prior reports had observed a strong narrow feature which we label band F; using similar arguments as made here for assigning peak D, this was assigned to the $A\,^5\Sigma^+ \leftarrow X\,^4\Delta$ transition [9–12]. Moreover, the ZEKE spectra observed no intensity for these features, consistent with the assignment of detachment from the 1δ orbital (see above). However, by using an ion trap, we have greater control over ion internal energy, and have shown that this feature originates from an excited anion state. The threshold behaviour can be more thoroughly characterised by SEVI, and we obtain threshold intensities characteristic of δ orbital detachment only for peak D. The ZEKE spectra showed peaks consistent with our band E; these had been tentatively assigned to a forbidden $a\,^7\Sigma^+ \leftarrow X\,^4\Delta$ transition, but we show that this band is a fully allowed transition from the same anion $a\,^6\Sigma^+$ excited state.

Theoretical calculations predict three low-lying anion and neutral states; we have assigned two anion states and three neutral states. The leftover state is a $^6\Delta$ anion state. As discussed previously, there is no evidence for population of such a state in the room temperature spectra; there is minimal structure below peak A1, where structure from a $^5\Delta \leftarrow {}^6\Delta$ transition would be expected. The $^6\Delta$ state is clearly higher in energy than the $^6\Sigma^+$ state. However, under vibrationally hot ion conditions (Figure 3), ordered structure is visible below peak A1. Previous PE spectra have assigned this progression to hot bands of the $X\,^5\Delta \leftarrow X\,^4\Delta$ transition [9,12], but due to the small FC activity (Figure 5), simulated FC spectra even at temperatures of 3000 K have insufficient hot band structure to reproduce the experimental structure. While the experimental cold spectra exhibit more FC activity than the simulations, qualitatively, there still appears to be too much FC activity than can be explained by just hot vibrational bands. In contrast, the $^5\Delta \leftarrow {}^6\Delta$ transition is calculated to have an extended FC progression. The combination of these two could result in the observed structure, similar to how overlapping progressions led to different assignments of the $^5\Delta$ vibrational frequencies by photoelectron and optical spectroscopy [12]. Unfortunately, due to difficulties in acquiring high-resolution spectra in this region (see Section 3), we are unable to resolve different contributions to the progression. Hence, an excited $^6\Delta$ anion state may contribute to the spectra at low eBE in Figure 3, but without well-resolved spectra in this region, such an assignment is only speculative.

6. Conclusions

High-resolution PE spectra are obtained of FeO^- by a combination of SEVI spectroscopy and ion trapping and cooling. Although higher resolution spectra than ours have been obtained by ZEKE spectroscopy, the ion trap allows for finer control over initial ion conditions, allowing for spectra acquired at cold, intermediate, and vibrationally hot temperatures. The additional information gained allows us to clarify confusing aspects of previous PE spectra, and we show that some features were due to an anion excited state that was insufficiently quenched in previous experiments. We obtain relative energies of the two lowest anion and three lowest neutral states of FeO, along with vibrational frequencies of the neutral states. Furthermore, we reaffirm the assignment of the $^4\Delta$ anion ground state, which has been questioned in recent theoretical calculations.

The deceptively complex diatomic FeO has been difficult to understand experimentally and theoretically. Anion photoelectron spectroscopy is a convenient technique for accessing otherwise dark states of the neutral species, but if the electronic structure of the ion is also complex, significant thermal population of anion excited states can complicate the interpretation of the spectra. High-resolution techniques like SEVI can help disentangle contributions from various states of hot ions, but ion trapping and cooling permits better controlled cooling to the ground state or low-lying states, simplifying and increasing confidence in the resulting analysis.

Disclosure statement

No potential conflict of interest was reported by the author(s).

Funding

This work is funded by the Air Force Office of Scientific Research [grant number FA9550-12-1-0160] and the Defense University Research Instrumentation Program [grant number FA9550-11-1-0330]. Marissa L. Weichman thanks the National Science Foundation for a graduate research fellowship.

References

[1] D.W. Green, G.T. Reedy, and J.G. Kay, J. Mol. Spectrosc. **78**, 257 (1979).
[2] G.V. Chertihin, W. Saffel, J.T. Yustein, L. Andrews, M. Neurock, A. Ricca, and C.W. Bauschlicher, J. Phys. Chem. **100**, 5261 (1996).
[3] Y. Gong, M. Zhou, and L. Andrews, Chem. Rev. **109**, 6765 (2009).
[4] Y. Endo, S. Saito, and E. Hirota, Astrophys. J. **278**, L131 (1984).
[5] T. Kröckertskothen, H. Knöckel, and E. Tiemann, Mol. Phys. **62**, 1031 (1987).
[6] M.D. Allen, L.M. Ziurys, and J.M. Brown, Chem. Phys. Lett. **257**, 130 (1996).
[7] T.C. Steimle, D.F. Nachman, J.E. Shirley, and A.J. Merer, J. Chem. Phys. **90**, 5360 (1989).
[8] T.C. Steimle, J. Gengler, and P.J. Hodges, J. Chem. Phys. **121**, 12303 (2004).
[9] P.C. Engelking and W.C. Lineberger, J. Chem. Phys. **66**, 5054 (1977).
[10] J. Fan and L.-S. Wang, J. Chem. Phys. **102**, 8714 (1995).
[11] H. Wu, S.R. Desai, and L.-S. Wang, J. Am. Chem. Soc. **118**, 5296 (1996).
[12] G. Drechsler, U. Boesl, C. Bäßmann, and E.W. Schlag, J. Chem. Phys. **107**, 2284 (1997).
[13] B. Rosen, Nature **156**, 570 (1945).
[14] R.F. Barrow and M. Senior, Nature **223**, 1359 (1969).
[15] J.B. West and H.P. Broida, J. Chem. Phys. **62**, 2566 (1975).
[16] S.M. Harris and R.F. Barrow, J. Mol. Spectrosc. **84**, 334 (1980).
[17] A.S.C. Cheung, R.M. Gordon, and A.J. Merer, J. Mol. Spectrosc. **87**, 289 (1981).
[18] A.S.C. Cheung, N. Lee, A.M. Lyyra, A.J. Merer, and A.W. Taylor, J. Mol. Spectrosc. **95**, 213 (1982).
[19] A.W. Taylor, A.S.C. Cheung, and A.J. Merer, J. Mol. Spectrosc. **113**, 487 (1985).
[20] M. Barnes, M.M. Fraser, P.G. Hajigeorgiou, and A.J. Merer, J. Mol. Spectrosc. **170**, 449 (1995).
[21] A.J. Merer, Annu. Rev. Phys. Chem. **40**, 407 (1989).
[22] T. Andersen, K.R. Lykke, D.M. Neumark, and W.C. Lineberger, J. Chem. Phys. **86**, 1858 (1987).
[23] P.S. Bagus and H.J.T. Preston, J. Chem. Phys. **59**, 2986 (1973).
[24] M. Krauss and W.J. Stevens, J. Chem. Phys. **82**, 5584 (1985).
[25] M. Dolg, U. Wedig, H. Stoll, and H. Preuss, J. Chem. Phys. **86**, 2123 (1987).
[26] C. Bauschlicher, Jr., S. Langhoff, and A. Komornicki, Theor. Chim. Acta **77**, 263 (1990).
[27] C. Bauschlicher, Jr. and P. Maitre, Theor. Chim. Acta **90**, 189 (1995).
[28] M.F.A. Hendrickx and K.R. Anam, J. Phys. Chem. A **113**, 8746 (2009).
[29] C.N. Sakellaris, E. Miliordos, and A. Mavridis, J. Chem. Phys. **134**, 234308 (2011).
[30] G.L. Gutsev, S.N. Khanna, B.K. Rao, and P. Jena, J. Phys. Chem. A **103**, 5812 (1999).
[31] G.L. Gutsev, B.K. Rao, and P. Jena, J. Phys. Chem. A **104**, 5374 (2000).
[32] E.L. Uzunova, G.S. Nikolov, and H. Mikosch, ChemPhysChem **5**, 192 (2004).
[33] D.M. Neumark and W.C. Lineberger, J. Phys. Chem. A **113**, 10588 (2009).
[34] D.M. Neumark, J. Phys. Chem. A **112**, 13287 (2008).
[35] C. Hock, J.B. Kim, M.L. Weichman, T.I. Yacovitch, and D.M. Neumark, J. Chem. Phys. **137**, 244201 (2012).
[36] A. Osterwalder, M.J. Nee, J. Zhou, and D.M. Neumark, J. Chem. Phys. **121**, 6317 (2004).
[37] A.T.J.B. Eppink and D.H. Parker, Rev. Sci. Instrum. **68**, 3477 (1997).
[38] M.B. Doyle, C. Abeyasera, and A.G. Suits, NuACQ, (2012).
[39] B. Dick, Phys. Chem. Chem. Phys. **16**, 570 (2014).
[40] J.B. Kim, M.L. Weichman, T.I. Yacovitch, C. Shih, and D.M. Neumark, J. Chem. Phys. **139**, 104301 (2013).
[41] J. Cooper and R.N. Zare, J. Chem. Phys. **48**, 942 (1968).
[42] K.L. Reid, Annu. Rev. Phys. Chem. **54**, 397 (2003).
[43] C. Bartels, C. Hock, J. Huwer, R. Kuhnen, J. Schwöbel, and B. von Issendorff, Science **323**, 1323 (2009).
[44] A. Sanov, Annu. Rev. Phys. Chem. **65**, 341 (2014).
[45] J.B. Kim, C. Hock, T.I. Yacovitch, and D.M. Neumark, J. Phys. Chem. A **117**, 8126 (2013).
[46] I.T. Jolliffe, *Principal Component Analysis* (Springer, New York, 2002).
[47] J. Xie and R.N. Zare, J. Chem. Phys. **93**, 3033 (1990).
[48] A.D. Buckingham, B.J. Orr, and J.M. Sichel, Philos. Trans. R. Soc. A **268**, 147 (1970).
[49] V.A. Mozhayskiy and A.I. Krylov, ezSpectrum, (2009).
[50] E.P. Wigner, Phys. Rev. **73**, 1002 (1948).
[51] P.C. Engelking, Phys. Rev. A **26**, 740 (1982).
[52] J.R. Smith, J.B. Kim, and W.C. Lineberger, Phys. Rev. A **55**, 2036 (1997).
[53] D. Khuseynov, C.C. Blackstone, L.M. Culberson, and A. Sanov, J. Chem. Phys. **141**, 124312 (2014).
[54] C.M. Oana and A.I. Krylov, J. Chem. Phys. **131**, 124114 (2009).
[55] P.C. Engelking and W.C. Lineberger, Phys. Rev. A **19**, 149 (1979).
[56] R.R. Corderman, P.C. Engelking, and W.C. Lineberger, J. Chem. Phys. **70**, 4474 (1979).